Downscaling HARMONIE-AROME with Large-Eddy simulation

B.J.H. van Stratum, A.P. Siebesma, J. Barkmeijer, B. van Ulft

Downscaling HARMONIE-AROME with Large-Eddy Simulation

Bart van Stratum[*][†]*, Pier Siebesma*[#][*]*, Jan Barkmeijer*[*] *and*
Bert van Ulft[*]

[*]Royal Netherlands Meteorological Institute (KNMI)
[#]Delft University of Technology

[†]bart@vanstratum.com

Dutch *Offshore* *Wind* Atlas

Contents

1 | Introduction

Large-eddy simulation (LES) has traditionally mostly been used for idealised/academic studies of the atmospheric boundary layer. Due to increases in computational resources, and the increased complexity of LES models, it has now become feasible to explore the use of LES in a setup which is meaningful for numerical weather prediction. (NWP, e.g. Schalkwijk et al., 2015b; Heinze et al., 2017b).

The use of LES over models based on the Reynolds averaged Navier-Stokes (RANS) equations – like numerical weather prediction (NWP) models like HARMONIE-AROME (hereafter: HARMONIE) or IFS – offers several potential advantages. RANS based models typically operate on a (horizontal) resolution of $\mathcal{O}(1\text{-}10 \text{ km})$, on which processes like turbulent mixing or dry/shallow convection are unresolved, and thus require a sub-grid scale parameterisation. In contrast, LES typically operates on a resolution of $\mathcal{O}(10\text{-}100 \text{ m})$, thereby explicitly resolving the largest modes of turbulence and convection, eliminating the need of a turbulence/convection parameterisation. With increases in computational power, the resolution of RANS models is slowly moving towards the resolution of LES. However, as the resolution of these models is increased, they slowly approach the (convective) *"grey zone"*, in which turbulence and convection are partially resolved and partially a sub-grid scale process, which remains a challenging area for NWP models (e.g. Tomassini et al., 2017).

In this report we build on previous work by e.g. Neggers et al. (2012); Schalkwijk et al. (2015a); Heinze et al. (2017a) by directly downscaling a mesoscale model with LES, thereby bypassing the *"grey zone"* altogether. In the Dutch Offshore Wind Atlas (DOWA) project[1], we explored two new methods to nest LES in the HARMONIE model:

---

[1] www.dutchoffshorewindatlas.nl

1. For relatively <u>small LES domains</u> of $\mathcal{O}(10 \text{ km})$, in which the mean atmospheric state varies little across the LES domain, we used a similar methodology as Neggers et al. (2012); Schalkwijk et al. (2015a); Heinze et al. (2017a), and prescribe the influence of large-scale processes like the advection of scalars and momentum, subsidence, and the influence of horizontal pressure gradients, as horizontally mean tendencies in the prognostic LES equations. However, where the previous studies relied on estimating these individual terms offline from the routine output of a mesoscale or global weather model, we modified HARMONIE to directly output the dynamic tendencies from its dynamic core, thereby fully utilising the strengths of a well-tuned NWP model.

2. For <u>large LES domains</u> of $\mathcal{O}(100 \text{ km})$, the mean atmospheric state can vary significantly across the LES domain, making it difficult to apply the previous method. For such an LES setup, we explored the use of a nesting method where the lateral boundaries of the LES model are nudged towards the HARMONIE fields (e.g. Davies, 1976), similar to the nesting of HARMONIE in e.g. the IFS model. Combining our (from origin) academic LES models with this approach introduces several challenges, like combining the lateral boundary relaxation with the cyclic boundaries in LES, and reducing the spinup of turbulence near the inflow boundaries.

We start in Chapter 2 with the work on the small domain LES, describing both the traditional methods from literature and our new approach, followed by the results/validation of a two week LES experiment over Cabauw. In Chapter 3 we discuss the explorative work on the large domain LES with lateral boundary nudging, including an idealised study on the inflow spinup of turbulence, followed by the first results of nesting LES in HARMONIE. Both chapters contain a section describing the archiving and availability of both the model setup and data.

2 | *Small domain LES*

2.1 | *Introduction*

This chapter describes the small domain LES downscaling work done by KNMI within the DOWA project. It starts with an overview of the traditional and new innovative downscaling methodologies, followed by the results of a two week validation over Cabauw, and finally a description of the code and data availability and archiving.

2.2 | *Downscaling methodologies*

For relatively small LES domains of $\mathcal{O}$(1-10 km), the large-scale variability within the LES domain can be assumed to be negligible. However, such small LES domains are influenced by larger-scale weather patterns through the advection of e.g. heat, moisture and momentum, large-scale vertical motions (subsidence), and horizontal pressure gradients, which need to be prescribed to the LES model as external forcings.

In the traditional method of LES downscaling, these external forcings are calculated from the three-dimensional (3D) routine output of a host NWP model. Following Schalkwijk et al. (2015a), the large-scale terms for an arbitrary scalar ψ can be defined as:

$$\left.\frac{\partial \widetilde{\psi}}{\partial t}\right|_{\text{LS}} = -\underbrace{\left\langle u_j^{\text{LS}}\frac{\partial \psi^{\text{LS}}}{\partial x_j}\right\rangle}_{\text{advection}} - \underbrace{\left\langle w^{\text{LS}}\right\rangle\frac{\partial \widetilde{\psi}}{\partial z}}_{\text{subsidence}} + \underbrace{\frac{1}{\tau_{\text{n}}}\left(\left\langle \psi^{\text{LS}}\right\rangle - \left\langle \widetilde{\psi}\right\rangle\right)}_{\text{relaxation}} + \underbrace{\left\langle F_\psi^{\text{LS}}\right\rangle}_{\text{sources}} \tag{2.1}$$

where all variables with a tilde are (filtered) LES variables, variables with a superscript LS are fields from the host model, and the angle brackets $\langle ... \rangle$ indicate a horizontal averaging operator over the size of the LES domain. The first term on the

right hand side is the large-scale advection, the second term is the interaction between large scale subsidence and the LES field, the third term is a relaxation of the mean state of LES to the state of the host model, and the last term contains optional sources or sinks. The relaxation time scale τ_n is typically set to a few hours, such that the LES model can develop with some freedom, without drifting too far from the state of the host model (Neggers et al., 2012).

For momentum, the large-scale terms are similar, with the addition of rotation (Coriolis term):

$$\frac{\partial \widetilde{u}_i}{\partial t}\bigg|_{\text{LS}} = -\underbrace{\left\langle u_j^{\text{LS}} \frac{\partial u_i^{\text{LS}}}{\partial x_j} \right\rangle}_{\text{advection}} - \underbrace{\left\langle w^{\text{LS}} \right\rangle \frac{\partial \widetilde{u}_i}{\partial z}}_{\text{subsidence}}$$

$$+ \underbrace{\epsilon_{ij3} f_c \left(\widetilde{u}_j - \left\langle u_{g;j}^{\text{LS}} \right\rangle \right)}_{\text{coriolis}} + \underbrace{\frac{1}{\tau_n} \left(\left\langle u_i^{\text{LS}} \right\rangle - \left\langle \widetilde{u}_i \right\rangle \right)}_{\text{relaxation}} + \underbrace{\left\langle F_{u_i}^{\text{LS}} \right\rangle}_{\text{sources}} \quad (2.2)$$

where $f_c = 2\,\Omega \sin(\phi)$ is the Coriolis frequency, with $\Omega = 7.2921 \cdot 10^{-5}$ rad s^{-1} and ϕ the latitude in radians, and u_g the geostrophic wind. Eq. 2.2 is only applied to the horizontal velocity components ($i = (1,2)$).

The terms from Eqs. 2.1 and 2.2 effectively reconstruct the tendencies from the dynamic core of the host model, but often in a simplified way. For example, HARMONIE calculates the advective tendencies using a semi-Lagrangian advection scheme in spectral space (Bengtsson et al., 2017), whereas the offline reconstruction typically uses a (less accurate) second order accurate finite difference method. In addition, this method results in instantaneous tendencies, only available at the output frequency of the host model, and intermediate events may be lost.

As an alternative, Eqs. 2.1 and 2.2 can be replaced by the actual tendencies from the dynamic core of the host model. As part of the DOWA project, we modified HARMONIE to output these dynamic tendencies. In practise, it proved difficult to directly extract the dynamic tendencies, so the dynamic tendencies are calculated as the difference between the total and physics tendencies – both of which could easily be isolated inside the HARMONIE code:

$$\frac{\partial \psi^{\text{LS}}}{\partial t}\bigg|_{\text{dyn}} = \frac{\partial \psi^{\text{LS}}}{\partial t}\bigg|_{\text{tot}} - \frac{\partial \psi^{\text{LS}}}{\partial t}\bigg|_{\text{phys}} \quad (2.3)$$

and similar for the velocity components. As a result, the dynamic tendency contains

4

the full model tendency from HARMONIE, minus the processes which are either resolved (e.g. turbulent mixing, convection) or parameterised (e.g. radiation, microphysics) by the LES model itself. The dynamic tendencies are accumulated in time inside HARMONIE, such that the full dynamic tendency is available for LES. These new dynamic tendencies simplify Eqs. 2.1 and 2.2 to:

$$\left.\frac{\partial \widetilde{\psi}}{\partial t}\right|_{\mathrm{LS}} = \left\langle \left.\frac{\partial \psi^{\mathrm{LS}}}{\partial t}\right|_{\mathrm{dyn}} \right\rangle + \frac{1}{\tau_{\mathrm{n}}} \left(\langle \psi^{\mathrm{LS}} \rangle - \langle \widetilde{\psi} \rangle \right) \tag{2.4}$$

$$\left.\frac{\partial \widetilde{u}_i}{\partial t}\right|_{\mathrm{LS}} = \left\langle \left.\frac{\partial u_i^{\mathrm{LS}}}{\partial t}\right|_{\mathrm{dyn}} \right\rangle + \frac{1}{\tau_{\mathrm{n}}} \left(\langle u_i^{\mathrm{LS}} \rangle - \langle \widetilde{u}_i \rangle \right) \tag{2.5}$$

The relaxation terms are kept in place, again to prevent LES from drifting from HARMONIE. Like with the traditional method, Eq. 2.5 is only applied to the horizontal velocity components in LES.

2.3 | Data availability

As part of the DOWA HARMONIE reanalysis (Wijnant et al., 2019), we generated three years of dynamic tendencies. For 2016 and 2017, these tendencies – including vertical profiles of the atmospheric state variables necessary for the initialisation and relaxation – are available for selected locations at a 10 minute interval, as a single model column, and horizontally averaged over $10{\times}10$ km^2 and $30{\times}30$ km^2. The locations were chosen based on interest and/or available observations, and are shown in Fig. 2.1.

For 2018, the dynamic tendencies are available at a one hour interval, for a $542.5{\times}585$ km^2 area covering the Netherlands and part of the North-sea. These files provide more flexibility in the choice of location and/or averaging area. Additional data required for the initialisation and/or relaxation is available from the default HARMONIE reanalysis dataset (Wijnant et al., 2019).

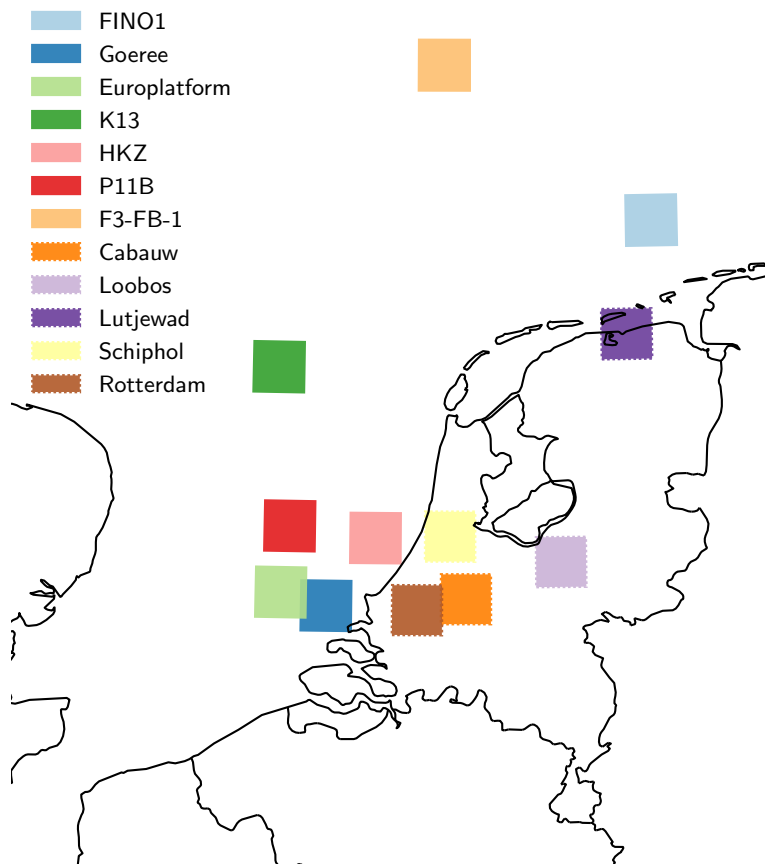The archiving of these data sets is described in Section 2.5.

Figure 2.1: Output locations (30×30 km^2) for the 2016-2017 dynamic LES tendencies from HARMONIE

2.4 | Validation

As a first validation of the new downscaling method using the dynamic tendencies from HARMONIE, we used DALES to simulate a two week period of realistic weather over Cabauw (51.97° N, 4.90° E). The period, from 04-08-2016 00 UTC to 18-08-2016 00 UTC, contained an interesting mix of weather phenomena, from clear convective boundary layers to precipitating frontal passages.

2.4.1 | Model description

The LES experiments were performed with DALES (Heus et al., 2010), using the RRTMG radiative transfer solver (Mlawer et al., 1997), a modified version of ECMWF's HTESSEL land-surface model (van Heerwaarden, 2011; van Tiggelen, 2018), and a

double moment warm microphysics scheme (Seifert & Beheng, 2001). Sub-grid diffusion was handled by the Deardorff TKE scheme (Deardorff, 1973), and advection of scalars, momentum and sub-grid TKE with a centered scheme using 5th (2nd) order accurate interpolations in the horizontal (vertical) (Wicker & Skamarock, 2002).

The domain was setup using a horizontal grid spacing of 78.125 m (192×192 grid points; 15×15 km), with a vertical grid stretched from 20 m near the surface to 150 m at ∼13500 m (160 grid points). To reduce the turnover time of the experiments, each day was simulated individually (in parallel), with a cold start at 00 UTC and a 24 hour time integration. For each individual day, the LES domain was initialised horizontally homogeneous from the 10x10 km^2 averaged HARMONIE output.

A switch of soil/land-surface scheme (in our case, from SURFEX in HARMONIE to HTESSEL in DALES) often results in a long spinup, as the land surface and especially the soil adjust to differences in the parameterisation and soil/surface properties (e.g. Angevine et al., 2014). Early experiments with the soil moisture and temperature initialised from HARMONIE revealed that without a propper spinup, the surface flux partitioning (sensible, latent and soil heat fluxes) was very poor compared to observations. Therefore, we chose to initialise the soil quantities from ERA5, which (without a spinup period) resulted in a good agreement of the surface fluxes in DALES with observations. Like the atmosphere, the soil and surface was initialised horizontally homogeneous.

To aid the comparison with observations, DALES was extended with an option to output statistics from individual grid points or columns (*virtual observation sites*). The statistics were sampled every 10 seconds and averaged over a 10 minute period, to mimic a point (or column) observation in reality.

2.4.2 | Results

Figure 2.2 shows the comparison between the LES results and Cabauw observations, for the 10 m and 200 m absolute wind speed. Overall, LES captures both the daily cycle (most clearly visible in the 10 m wind speed) and inter-day variability well, but slightly overestimates the wind at both heights. At 10 m height, the mean error (defined here as model minus observation) is 0.4 m s^{-1}, and 0.6 m s^{-1} at 200 m height. A plausible cause for this difference is the roughness length for momentum (z_{0m}). In LES, z_{0m} is set to 7.5 cm, higher than the local roughness of the grassland (z_{0m} = 3 cm), but for several wind sectors lower than the regional roughness length (Bosveld, 2019). The use of more realistic (spatially and/or time varying) surface properties might improve these results.
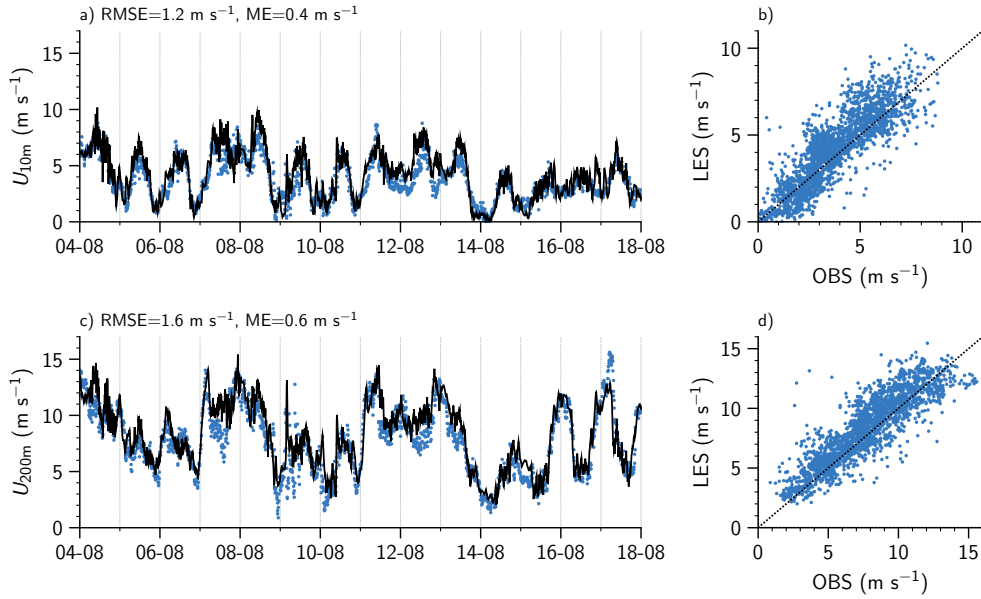
Figure 2.2: Comparison LES (lines) and Cabauw measurements (dots) for the 10 m and 200 m wind speed.

The 10 m and 200 m temperature and specific humidity are shown in Fig. 2.3 and 2.4. As for wind speed, both the intra and inter-day variability is well reproduced by LES. At 10m height, the maximum daytime temperatures are in line with the observations, only on a few nights the the minimum temperature in LES is underestimated by 2-3 degrees, resulting in a mean bias of -0.3 degrees. The 10 m specific humidity is underestimated as well (both during day and night), with a mean bias of -0.4 g kg^{-1}. Both the 200 m temperature and specific humidity are overall in line with the observations, with a mean bias close to zero.

We next focus on the surface energy balance (SEB), with the surface radiation and surface heat and moisture fluxes. Fig. 2.5 shows the incoming and outgoing long and shortwave radiation, compared to the Cabauw observations. The shortwave incoming radiation is – on average – well represented in LES, only on relatively cloudy days (like 04-08 and especially 11-08) the incoming radiation is underestimated. Despite the use of the *virtual observation sites* in LES, the short-term variability in incoming shortwave radiation seems to be underestimated. The incoming longwave radiation is in good agreement with the observations. The outgoing longwave radiation underestimates the extremes during both day and night, underestimating the daytime outgoing radiation, and overestimating the nighttime outgoing radiation. This seems to indicate that the amplitude of the surface temperature is underestimated by LES.

The surface energy partitioning, with the net surface radiation (Q_{net}) distributed
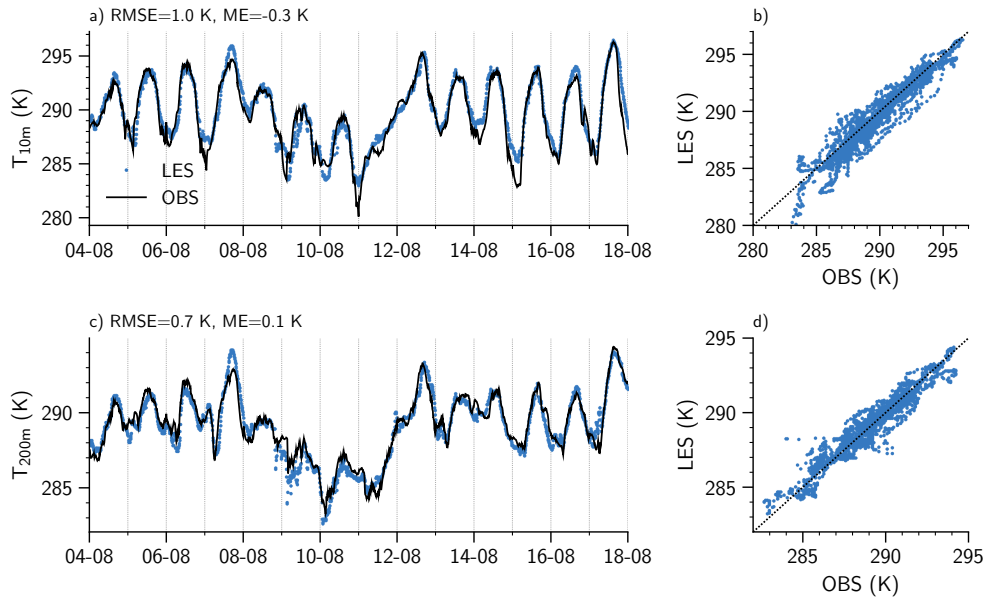
*Figure 2.3: Comparison LES (lines) and Cabauw measurements (dots) for the
10 m and 200 m temperature*

over the sensible (H), latent (LE) and soil (G) heat fluxes, is shown in Fig. 2.6. The
surface fluxes are in reasonable agreement with the observations. On days where the
incoming shortwave radiation is underestimated, the sensible and latent heat fluxes
are underestimated as well, as the result of a shortage of available energy (Q_{net}).
During daytime, a small shift is visible from the latent to sensible heat flux, with an
underestimation of evaporation, and overestimation of the sensible heat flux. During
the night, the negative evaporation (dew deposition) is often absent or (in absolute
sense) too small in LES, which contradicts the underestimation of the nighttime spe-
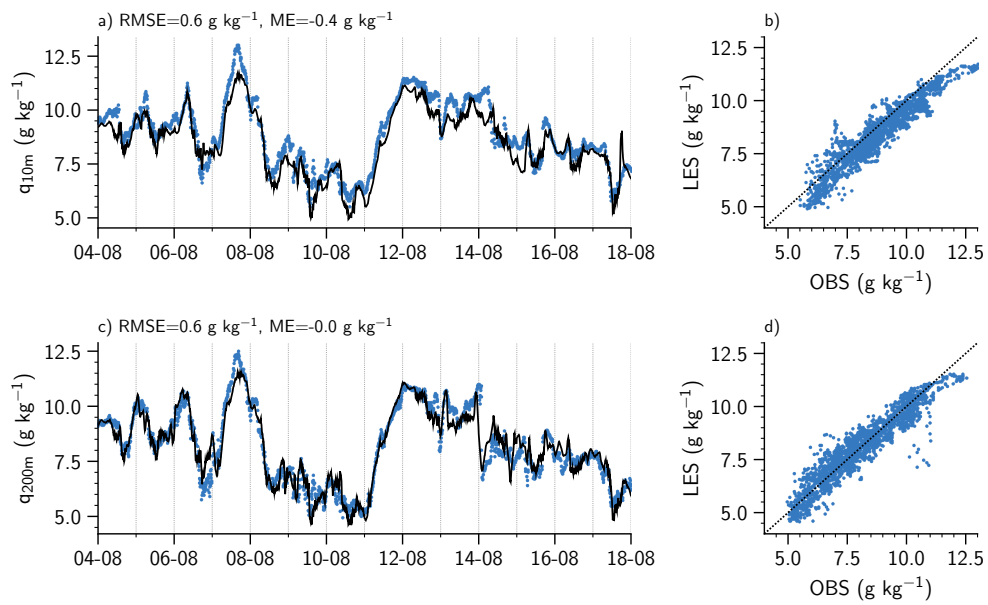cific humidity (Fig. 2.4).

Figure 2.4: Comparison LES (lines) and Cabauw measurements (dots) for the 10 m and 200 m specific humidity
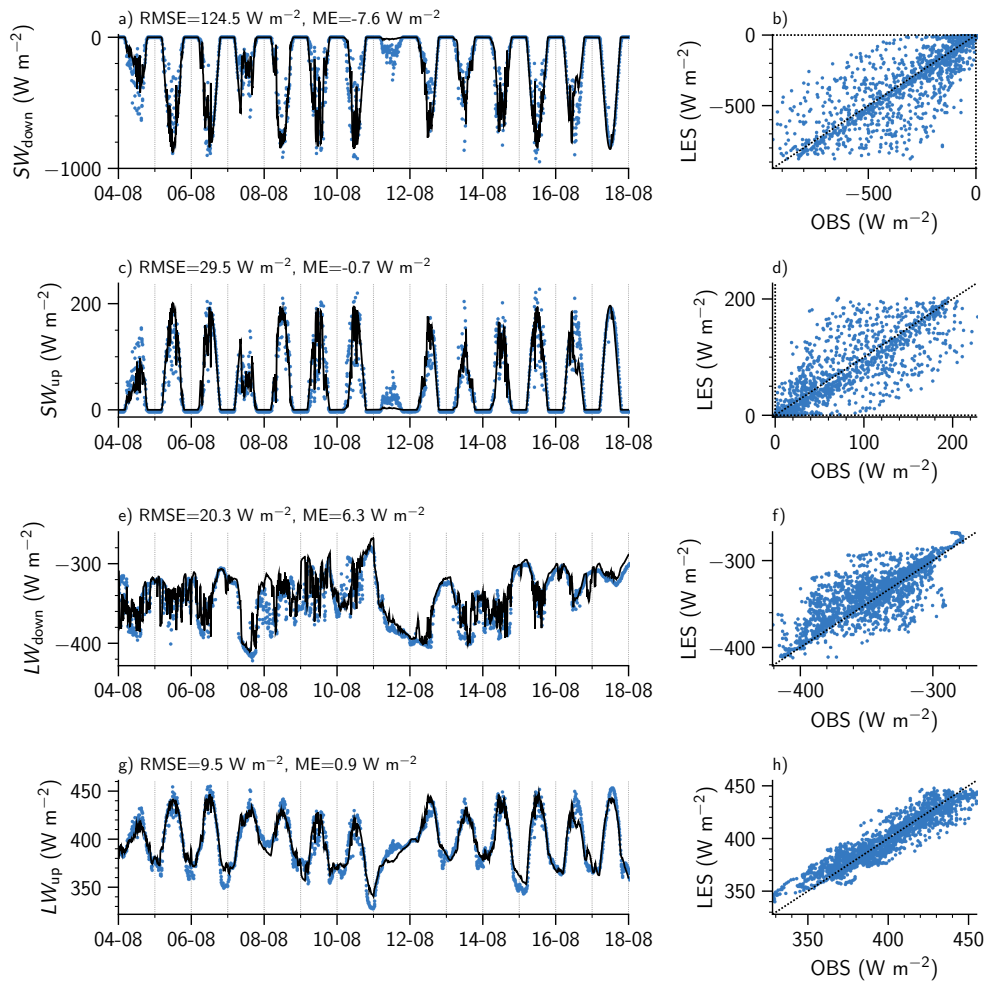
Figure 2.5: Surface radiation balance Cabauw, comparing LES (black line) with the Cabauw observations (dots). All fluxes are defined as being positive upwards.
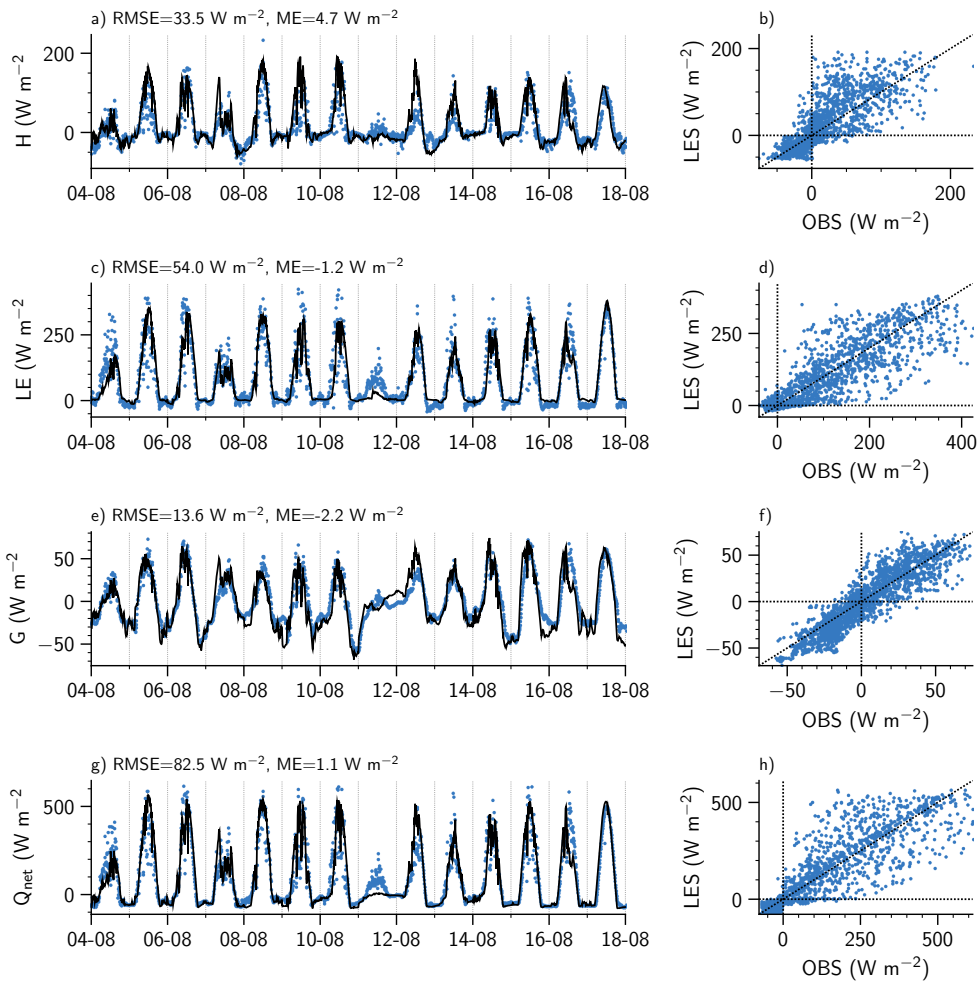
Figure 2.6: Surface energy balance Cabauw, comparing LES (black line) with the Cabauw observations (dots). All fluxes are defined as being positive upwards.

2.5 | Archiving

The modified HARMONIE code used to generate the dynamic tendencies is archived at the KNMI Gitlab account:

2016: `https://gitlab.com/KNMI/RDWK/dowa/dowa_hm_home/tree/master/DOWA_40h12tg2_fERA5_ptE`

2017: `https://gitlab.com/KNMI/RDWK/dowa/dowa_hm_home/tree/master/DOWA_40h12tg2_fERA5_ptD`

2018: `https://gitlab.com/KNMI/RDWK/dowa/dowa_hm_home/tree/master/DOWA_40h12tg2_fERA5_ptF`

The data (dynamic tendencies) are stored in the ECMWF tape archive:

2016-2017: `ec:/nkl/harmonie/DOWA/DOWA_40h12tg2_fERA5/LES_forcing`, available in compressed monthly batches of daily NetCDF files.

2018: `ec:/nkl/harmonie/DOWA/DOWA_40h12tg2_fERA5/ptF_2018`, available as monthly NetCDF files. All relevant files/variables are named `dtX_dyn`, with $X = T$ (temperature), `q` (specific humidity) or `u,v` (horizontal wind components).

The DALES case setup is archived at: `https://github.com/julietbravo/KNMI_testbed/tree/master/cases/cabauw`. A slightly modified version of DALES is required to work with the dynamic tendencies from HARMONIE, available at: `https://github.com/julietbravo/dales/tree/to4.2_knmi_testbed`.

2.6 | Conclusions

This chapter described the small domain LES downscaling work done by KNMI. The main outcomes are (1) the availability of a modified version of HARMONIE which can calculate and output the dynamic model tendencies, and (2) the production of three years of dynamic tendencies from the DOWA/HARMONIE reanalysis.

As a first validation of the new downscaling method using the dynamic tendencies from HARMONIE, we used DALES to simulate a two week period of realistic weather over Cabauw. Overall, the results are in good agreement with the Cabauw observations, and LES reproduced both the intra and inter-day variability of the realistic weather well.

In the DOWA project, the full validation – comparing the traditional and new downscaling methods for long time series – was performed by Whiffle.

3 | *Large domain LES*

3.1 | *Introduction*

The downscaling methodology described in Chapter 2 is useful for LES on relatively small domains of $\mathcal{O}$(1-10 km), where the mean atmospheric state varies little across the LES domain. For larger domains of $\mathcal{O}$(100 km), in which the mean large-scale state can vary significantly, a different approach is adopted. This approach is similar to the nesting method of limited area models (like e.g. HARMONIE in IFS), where the lateral boundaries of the model are nudged towards the fields of a host model.

3.2 | *Inflow methodology*

The lateral boundary nudging or relaxation is essentially a local blending between an external field from the host model (ϕ^{LS}) and a local model field (ϕ):

$$\phi_{t+1} = f_n \phi_t^{\text{LS}} + (1 - f_n)\, \phi_t, \tag{3.1}$$

where f_n (range 0-1) controls the blending. In most mesoscale models, the logical choice is to set f_n=1 at the edges of the domain, f_n=0 in the interior, smoothly varying in between (e.g. Radnóti, 1995). However, in our case, this approach causes problems because of the use of cyclic boundaries in LES.

This problem is illustrated in Fig. 3.1, where an LES field (constant in space) is blended with a large-scale field which has a mean gradient through the LES domain. When blended with f_n=1 at the lateral boundaries (dashed red line), a large difference in ϕ between the left and right boundaries is introduced. Seen through the cyclic boundaries, this difference is a large discontinuity in the LES fields, which is likely to cause issues with e.g. advection. When blended with f_n=0 at the lat-

eral boundaries and f_n=1 at some distance from the boundaries, this discontinuity is smoothed out (blue dashed line).
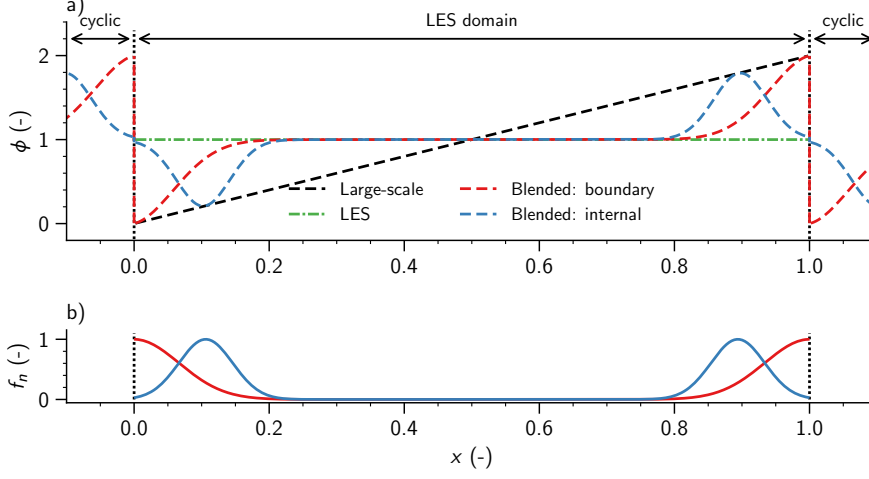

Figure 3.1: Illustration of combining the lateral boundary nudging with cyclic boundaries in LES.

This problem could altogether be avoided by removing the cycling boundaries from LES. However, this would require the implementation of a different pressure solver in LES (which does not rely on a fast Fourier transform (FFT)), which is beyond the scope of this project. To study cases with lateral boundary relaxation, we therefore chose to apply the lateral boundary relaxation at some distance from the cyclic boundaries – as shown in Fig. 3.1b (blue line) – with f_n as a simple Gaussian function, defined as:

$$f_n = \exp\left(-\frac{1}{2}\left(\frac{(x - x_c)}{\sigma}\right)^2\right),\qquad(3.2)$$

where x_c is the center of the nudging area, and σ is the standard deviation, controlling the width of the nudging area.

In order to manipulate the LES tendencies instead of the LES fields, Eq. 3.1 is implemented in LES as:

$$\frac{\partial \widetilde{\phi}}{\partial t} = \frac{f_n}{\tau_b}\left(\phi_{ls} - \widetilde{\phi}\right),\qquad(3.3)$$

where τ_b is a nudging time scale. With $\tau_b = \Delta t$ (with Δt the model time step), Eq. 3.3 is equivalent to Eq. 3.1.

3.3 | Inflow turbulence generation

When nesting LES in a non-turbulence resolving model like HARMONIE, the LES requires some time to adjust from the non-turbulent inflow at the boundaries, to fully developed turbulence in the LES domain (spinup). Several methods exist to expedite the turbulence generation (see Wu, 2017, for a comprehensive review), for example using synthetic turbulence at the inflow boundaries (e.g. Muñoz-Esparza et al., 2014, 2015), or by recycling turbulence from the interior of the LES domain (e.g. Lund et al., 1998; Mayor et al., 2002; Nakayama et al., 2012).

In this project we tested two methods to reduce the turbulence spinup at the inflow boundaries: a synthetic turbulence method based on Muñoz-Esparza et al. (2014, 2015), and a modified version of the turbulence recycling method from Mayor et al. (2002).

3.3.1 | Synthetic turbulence

In the synthetic turbulence method from Muñoz-Esparza et al. (2014, 2015), the potential temperature field near the lateral boundaries is perturbed with random fluctuations. As small scale perturbations (perturbations at individual grid points) tend to dissipate quickly, the perturbations are added as blocks of $N \times N$ grid points in the horizontal plane, referred to as a cell perturbation method. The main difficulty lies in the choice of the magnitude of the perturbations, for example relating them to potential temperature variance scaling laws (e.g. Muñoz-Esparza & Kosović, 2018). As we only explored the inflow turbulence generation in an idealised setup (discussed later), we simply prescribed the potential temperature fluctuations.

The main advantage of the synthetic turbulence method over the turbulence recycling method, is that it is relatively easy, and can be applied to all lateral boundaries, independent of whether there is in- or outflow. The main disadvantage is that it can require a relatively long fetch before the random perturbations have developed into realistic turbulence.

3.3.2 | Turbulence recycling

The goal of the turbulence recycling method is – as the name implies – to recycle turbulence from areas with well (or at least better) resolved turbulence, to areas near the inflow boundaries where turbulence is mostly unresolved. This idea is sketched

in Fig. 3.2, where a variable ψ at some distance from the inflow boundary (source area S) is decomposed into its mean and fluctuating part: $\psi_S = \langle\psi\rangle_S + \psi_S'$. In Mayor et al. (2002), the fluctuating part ψ_S' was continuously added to a mean inflow profile $\langle\psi\rangle_G$, which they obtained from a another (precursor) experiment. We adopted a slightly modified version, where $\langle\psi\rangle_G$ is the horizontal mean (in some sensible direction, e.g. perpendicular to the flow direction) of the current LES experiment, and nudge the perturbations of the goal area towards the perturbations of the source area:

$$\frac{\partial \psi_G'}{\partial t} = \frac{1}{\tau_r}\left(\psi_S' - \psi_G'\right), \tag{3.4}$$

with τ_r as a nudging time scale. Both the location and width of the source and goal areas can be chosen freely, but the distance between the source and goal are should (ideally) be large enough to allow de-correlation of the turbulent fluctuations before they are recycled from the source to goal area.

The main advantage of the turbulence recycling method over the synthetic turbulence method, is that it can greatly reduce the spinup near the inflow boundaries. The main disadvantage is that it is difficult to generalise for complex inflow conditions.
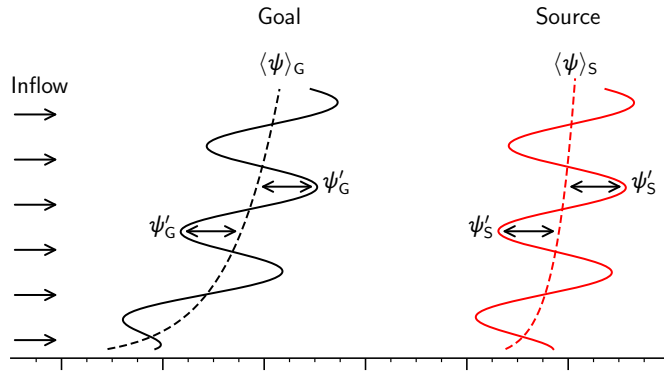

Figure 3.2: *Sketch of the turbulence recycling method, recycling the turbulent fluctuations from a source to goal area.*

3.4 | Idealised inflow test case

To study the spinup of turbulence at the lateral (inflow) boundaries, we setup an idealised experiment based on the BOMEX (*Barbados Oceanographic and Meteorological Experiment*) LES intercomparison (Siebesma et al., 2003). BOMEX was focussed on

non-precipitating trade wind cumulus. Being in a steady-state, the mean thermodynamic structure and turbulence statistics are constant in space and time, and can be used to validate the developing turbulent flow downstream of the inflow boundaries.

3.4.1 | Case setup

To simplify the setup and reduce the computational costs, the experiments were performed in a long rectangular domain of $60 \times 12 \times 3$ km^3, using a grid spacing of $\Delta x = \Delta y = 50$ m, $\Delta z = 40$ m, and a total time integration of 12 hours. The original BOMEX case starts as a purely zonal flow $[(u, v) = (\text{-}8.75, 0)$ m s^{-1} near the surface$]$, but develops a meridional component through rotation. To suppress the meridional component, rotation was disabled by setting the coriolis term in Eq. 2.2 to zero. Without the coriolis term the flow would slowly decelerate, which was prevented by continuously nudging the zonal wind component to the vertical profile from a reference (precursor) experiment.

The inflow velocity components (u, v, and w), liquid water potential temperature (θ_l) and specific humidity (q_t) are nudged to the domain averaged profiles of each quantity. This way, the inflow conditions are laminarised, without affecting the mean state of the LES experiment.

Several experiments were performed to study the inflow spinup of turbulence, which will be introduced alongside with the results. Some of the common settings related to the lateral boundary nudging, inflow perturbations, and turbulence recycling, are shown in Fig. 3.3. The lateral boundary nudging parameter f_n was centred around $x = 500$ m, with a width of $\sim$1000 m. The inflow potential temperature perturbations (± 0.125 K, multiplied with a perturbation factor f_p) were applied just downstream of the boundary nudging, centred around $x = 1000$ m. The turbulence recycling method used a source area of 1000 m wide, starting at $x = 8500$ m, with a
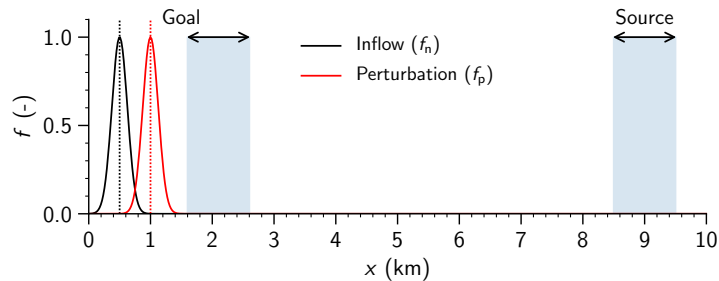

Figure 3.3: Details of the inflow nudging, perturbation, and turbulence recycling method.

goal area starting at $x = 1600$ m. The goal area was deliberately positioned further downstream of the inflow region, to allow for experiments with both the perturbations and turbulence recycling (a setup which is not further used or discussed in this report).

3.4.2 | Results

Figure 3.4 starts with a comparison of the cloud field, showing spanwise (y-direction) averaged $x - z$ cross sections of the liquid water specific humidity, at $t = 12$ hours.

a) The top panel shows a reference experiment, with the modified BOMEX case, without any treatment of the inflow conditions (i.e. normal cycling boundaries).

b) The second panel shows an experiment where the inflow profiles are nudged towards the domain mean profiles, without applying the perturbation or turbulence recycling method. It takes ~15 km before the first clouds are formed, followed by an area of ~10 km with intense convection, with weaker convection behind. Overall, it requires ~30-40 km before the results (visually) converge with the reference experiment.

c) The third panel shows the results with the inflow perturbations applied, in horizontal blocks of 10×10 grid points. Even these relatively simple perturbations strongly reduce the spinup, with the first clouds forming after ~5 km. However, as shown later, more detailed turbulence statistics still require a much longer distance to converge to the reference case.

d) Finally, the fourth panel shows the results from the turbulence recycling method. Almost directly from the recycling goal area, the cloud field shows a good resemblance with the reference experiment.

As a more strict validation, we next compare the vertical velocity variances, calculated over the spanwise direction:

$$\langle \sigma_w^2 \rangle_y = \langle (w - \langle w \rangle_y)^2 \rangle_y \tag{3.5}$$

The variances were averaged over the last 10 hours of the experiments. Figure 3.5 shows the variances at $z = 100$ m, $z = 300$ m (middle of the sub-cloud layer), and $z = 700$ m and $z = 1000$ m (bottom of the cloud layer). By design, the variance of the reference case is constant in the streamwise direction, which acts as a reference for the other three cases. Close to the surface, the case with the laminar inflow requires
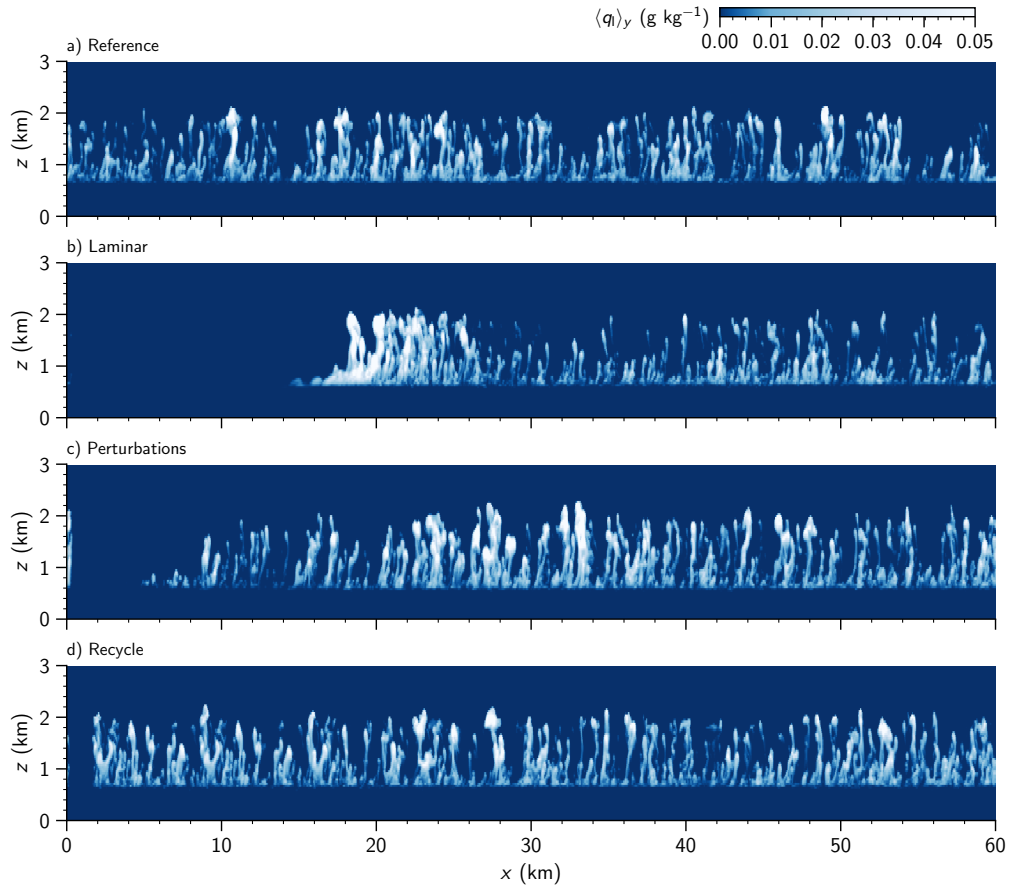
20

Figure 3.4: Vertical cross section of the spanwise (y-direction) averaged liquid water specific humidity at t=12 hours.

~10 km before turbulence develops, which increases to >15 km higher up. This laminar regime is followed by an area where the vertical velocity variance is strongly overestimated, which takes up to 30 km to decay and converge with the reference experiment. At a height of 100 m, the case with the inflow perturbations quickly converges with the reference experiment. However, higher up, the vertical velocity variance is first underestimated, and later overestimated, which takes >30 km to converge with the reference case at $z = 1000$ m. At all heights, the experiment with the turbulence recycling quickly converges with the reference experiment, although the variance is (for most heights) slightly overestimated in the first 15 km.

Finally, to examine the transition from the inflow nudging to realistic turbulence, Fig. 3.6 shows horizontal cross sections of the vertical velocity at $z =40$ m and $z =240$ m height. The top row (a, b) shows the reference experiment, the second row (c, d) the experiment with the laminar inflow, the third row (e, f) the experiment with random perturbations, and the bottom row (g, h) the experiment with turbulence recycling. Once turbulence develops in the case with the laminar inflow, it is mostly
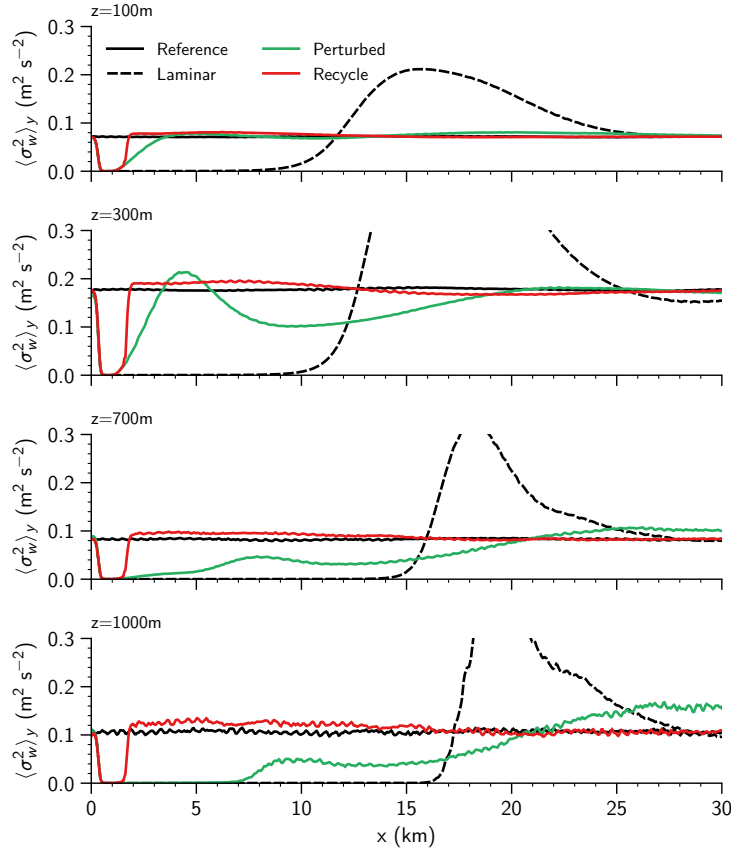
Figure 3.5: Spanwise calculated vertical velocity variances, averaged over the last 10 hours of the experiments.

in the form of long streaky patterns. The experiment with random perturbations requires ∼10 km before the blocked patterns from the perturbations disappear, and realistic turbulent structures are formed. As in the previous figures, the experiment with the turbulence recycling produces realistic turbulence directly from the goal area of the recycling method. However, as a result of the recycling method, series of similar spatial structures appear, spaced ∼7 km (the distance between the source and goal areas) apart. This could possibly be improved by increasing the distance between the source and goal area, allowing for a better de-correlation of the turbulent structures before recycling them from the source to goal area.
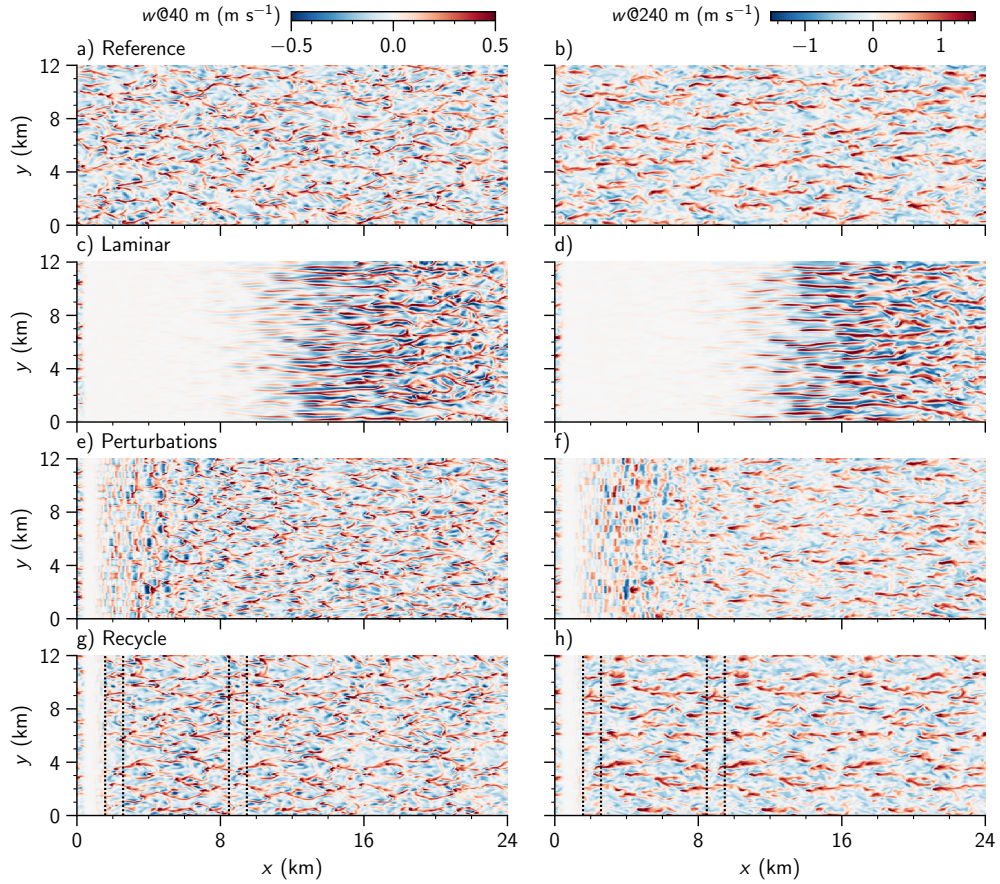
Figure 3.6: Horizontal cross sections of the vertical velocity at 40 m and 240 m height, at t=12 hours.

3.5 | Nesting LES in HARMONIE

As a proof of concept of the new nesting method with the lateral boundary nudging, we nested DALES into the HARMONIE model. The setup from the previous section – where the boundary nudging was only applied at the inflow (west) boundary – was extended to all four lateral boundaries, where data from the DOWA reanalysis was fed into DALES.

3.5.1 | Method and case setup

The setup of the LES experiments was relatively straightforward. Instead of initial-ising LES horizontally homogeneous – as is typically done with LES – the initial con-ditions were obtained by interpolating the HARMONIE fields onto the LES grid, con-verted into the prognostic quantities used by LES (liquid water potential temperature

23

θ_l, and total specific humidity q_t). For the data used by the lateral boundary nudging, the same procedure was repeated, interpolating the hourly data from HARMONIE onto the LES grid. To simplify the case setup, we only considered experiments over the North Sea, where we could set the lower boundary condition in LES to the (spatially varying) sea surface temperature (SST) from HARMONIE. To further simplify and generalise the procedure inside DALES, all interpolations from the host model grid to the LES grid were performed offline, such that an extension to other host models (e.g. IFS) is straightforward. The initial and (lower and lateral) boundary conditions are provided to DALES as binary files, the boundaries are linearly interpolated inside the LES model. The lower and lateral boundaries provide the only coupling between LES and HARMONIE, other options like e.g. (spectral) nudging of LES towards HARMONIE was not included in the experiments. Neither of the inflow turbulence generation techniques described in Section 3.3 were used in the experiments.

The LES domain (336×336 km) was positioned over the North Sea (Fig. 3.7), using 1680×1680 grid points in the horizontal, and 128 grid points in the vertical, starting with a grid spacing of 25 m near the surface, stretched up to a height of 11.15 km.
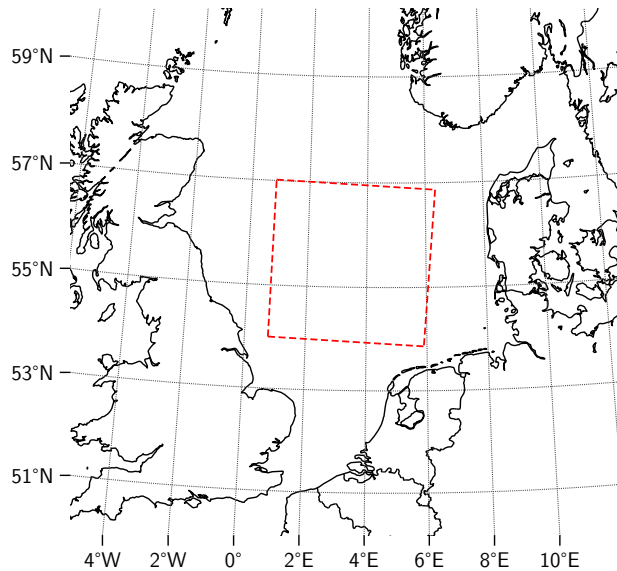

Figure 3.7: Location of the LES domain.

We should stress that these experiments should be seen as a proof of concept of the coupling between HARMONIE and LES at the lateral boundaries. These large domain LES experiments of realistic weather introduce several complexities which

are usually not present (or are neglected) in small domain LES experiments, like spatial variations in the surface and upper air pressure. The impact of large-scale pressure gradients and rotation is usually included in LES by specifying a spatially constant coriolis parameter (f-plane approximation) and geostrophic wind profile (Eq. 2.2); choices which are questionable on domains as large as 300 km. For simplicity, the LES experiments used a constant surface pressure set to the domain mean surface pressure from HARMONIE, and the entire coriolis term in Eq. 2.2 was set to zero. Furthermore, to reduce the computational costs, no interactive radiation was included, and microphysics was handled by the double moment warm microphysics scheme. These shortcomings will have to be addressed in future work, in order to obtain a more realistic representation of the complex nature of realistic weather.

The case considered here (7 September 2018, 08:00 to 14:00 UTC) was characterised by a low pressure area over the North Sea, with an occluded front in the northern part of our LES domain, as shown in Fig. 3.8. This resulted in a complex flow pattern, and a large meridional gradient in e.g. specific humidity, which – without the lateral boundary nudging – is difficult or impossible to contain in LES with cyclic boundaries.
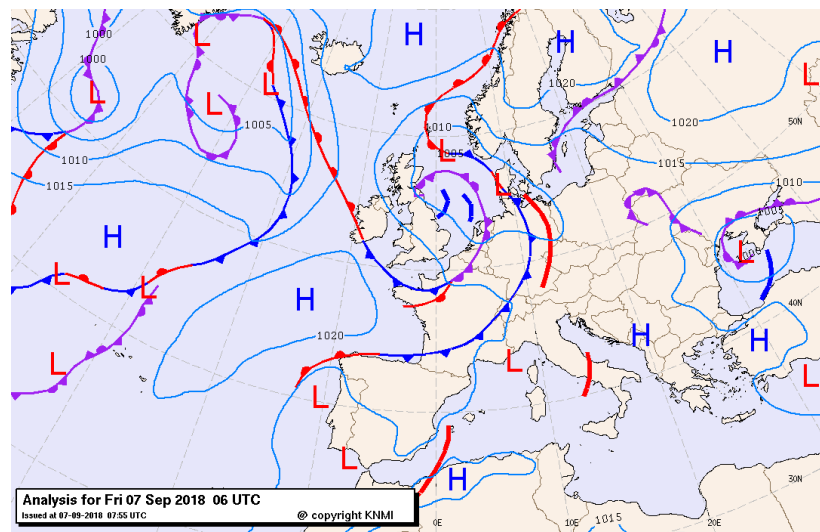

Figure 3.8: KNMI surface analysis for 07-09-2018 06:00 UTC, obtained from
https://www.knmi.nl/nederland-nu/klimatologie/daggegevens/
weerkaarten.

3.5.2 | Results

Figure 3.9 shows the wind field at 12.5 m height, in HARMONIE (left) and LES (right), at 14:00 UTC. The wind vanes are plotted every 8th grid point in HARMONIE,

and every 100th grid point in LES. Overall, the flow field from HARMONIE is reasonably well reproduced by LES, with weak winds in the NW part and stronger wind in the SE part of the domain, and a turning of the wind from westerly to south westerly. However, the absolute wind speed in LES is clearly higher in the SE part.
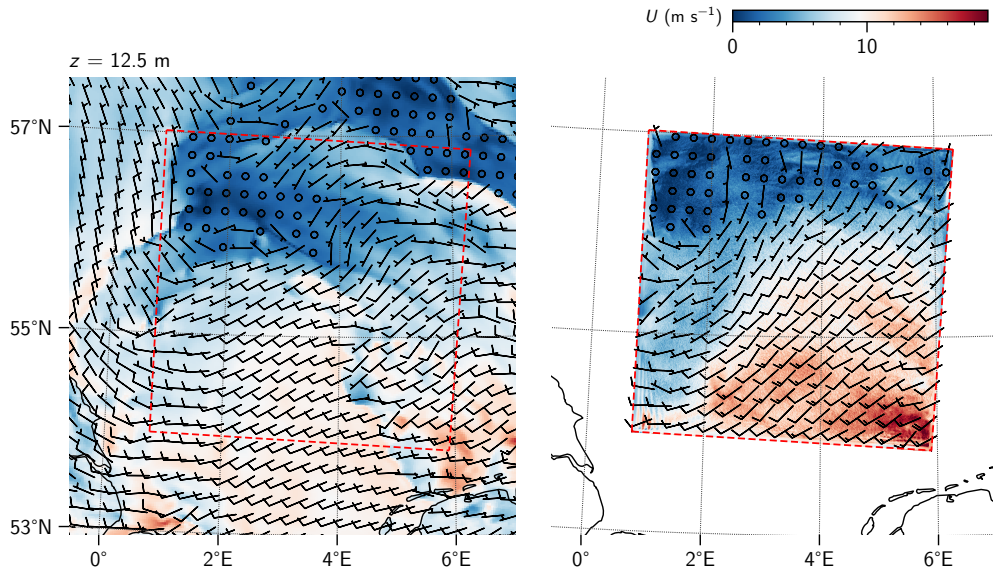

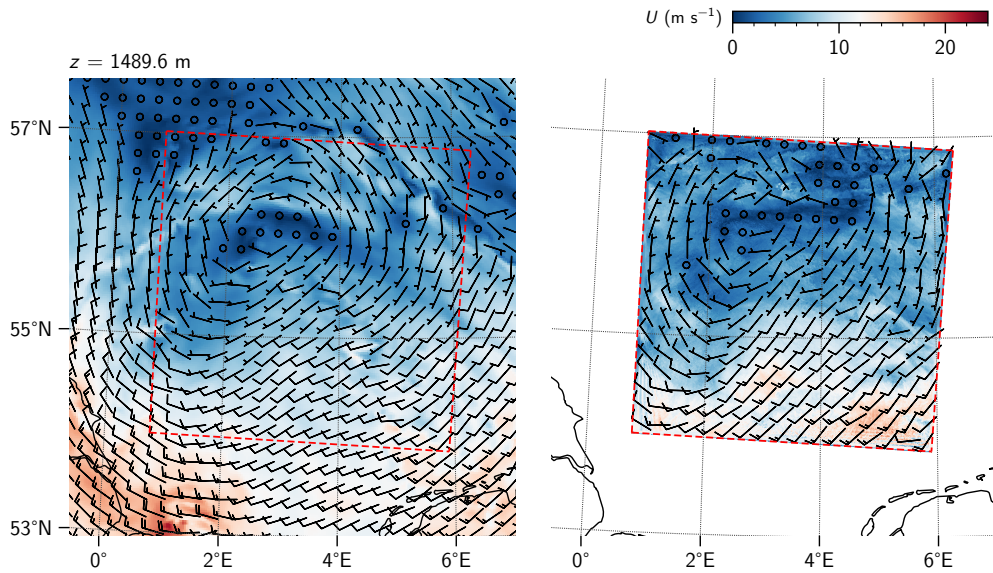Figure 3.9: Wind field at 12.5 m height, in HARMONIE (left) and LES (right).

Figure 3.10: Wind field at 1489.6 m height, in HARMONIE (left) and LES (right).

At ~1500 m height (Fig. 3.10) the depression is clearly visible, with a counter clockwise rotating flow around 3^oE, 56^oN. Despite the lack of a proper representation of the large scale dynamic processes, this complex flow pattern is well reproduced by

26

LES, perhaps simply because LES receives a rotating flow field at the lateral boundaries.

Figure 3.11 shows the specific humidity at 12.5 m height, with the data from LES (inside the red square) plotted over the HARMONIE data (outside the red square). The coupling between LES and HARMONIE is visible near the western boundary, where several moist plumes are advected from HARMONIE into LES. A relatively large meridional gradient is visible, with moist air in the northern part, and drier air in the south. Without the lateral boundary nudging, such gradients would eventually vanish as (depending on the wind direction) the cyclic boundaries would let the moist air enter in the south, or the dry air enter in the north. With the lateral boundary coupling, this meridional gradient is isolated from the cyclic boundaries.
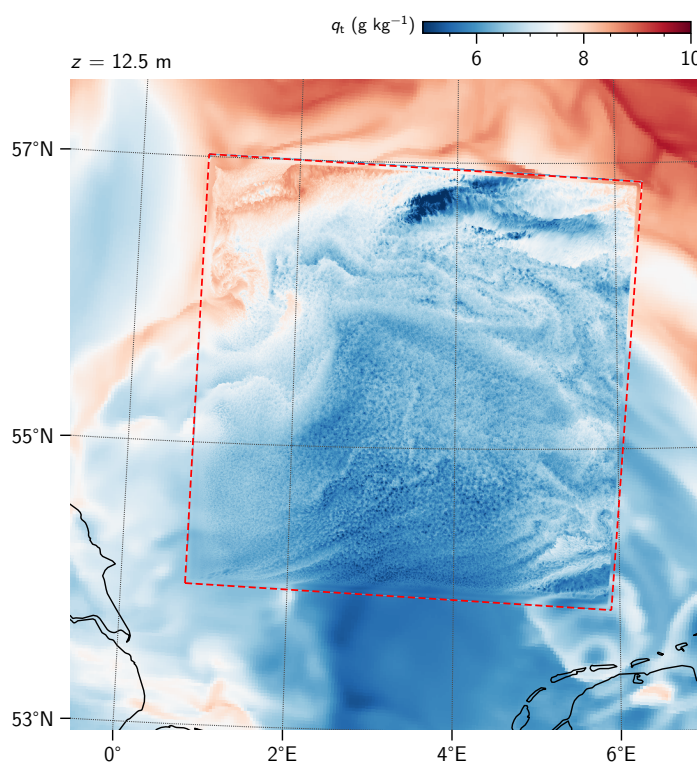

Figure 3.11: Specific humidity at 12.5 m height, with the LES data (red square) plotted op top of the HARMONIE data

Finally, Fig. 3.12 shows a comparison between the cloud field in LES and the MODIS (Moderate Resolution Imaging Spectroradiometer) Terra satellite image. The image from LES was obtained from the cloud liquid water path (LWP), converted into a synthetic albedo (Seifert & Heus, 2013):

$$\alpha = \frac{\tau}{6.8 + \tau}; \qquad \tau = 0.19 \, \text{LWP}^{5/6} \, N_c^{1/3}, \tag{3.6}$$

where N_c is the prescribed cloud droplet number mixing ratio (set to $300 \cdot 10^6$).

The occluded front is well visible in both LES and the satellite image, and the shallow moist convection south of the frontal area is resolved and captured by LES. However, the satellite image shows much larger cloud structures south of the occluded front, presumably some deeper and/or aggregated cloud systems, which are not present in LES.
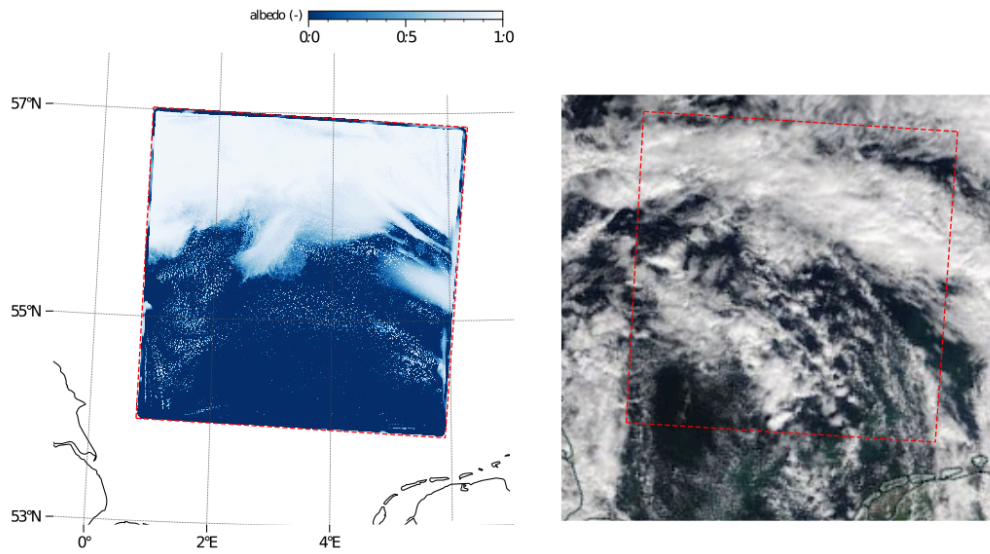

Figure 3.12: Synthetic albedo from LES (14:00 UTC, left), and the MODIS Terra image (~13:00 UTC, right). The LES domain in the right image is only intended as a visual guide.

3.6 | Archiving

The DALES case setup for the idealised experiments is archived at: `https://github` `.com/julietbravo/KNMI_testbed/tree/master/cases/nudge_boundary_bomex`, which requires a modified version of DALES, available at: `https://github.com/julietbravo/` `dales/tree/4.2_nudgeboundary_ideal`. The setup for the realistic experiments is archived at: `https://github.com/julietbravo/KNMI_testbed/tree/master/cases/` `nudge_boundary_HARMONIE`, and the DALES code at: `https://github.com/julietbravo/` `dales/tree/4.2_nudgeboundary`.

3.7 | *Conclusions*

This chapter described the explorative work done by KNMI on nesting large domain LES in models like HARMONIE.

As most of our (academic) LES models use cyclic boundaries, a variation on nesting with lateral boundary nudging was developed, which allows the use of lateral boundary nudging without interfering with the cyclic boundaries. This method allowed us to nest DALES in HARMONIE, without the need for extensive and complex changes in the DALES code.

The nesting of a turbulence resolving model like in LES in a non turbulence resolving model like HARMONIE, always results in some spinup of turbulence near the inflow boundaries. With an idealised test case, we explored several methods to reduce this spinup. The method with synthetic turbulence, which perturbs the inflow fields, provides a small improvement and reduction in the spinup, and is easy to incorporate in more complex and/or realistic cases. The method with turbulence recycling greatly reduces the spinup, but is more difficult to unite with complex in- and outflow patterns.

As a proof of concept, we demonstrated the nesting of DALES in the HARMONIE reanalysis. Despite the simple setup, this allowed us to introduce and contain a realistic case, with a (for LES standards) complex flow pattern, in LES.

References

Angevine, W. M., Bazile, E., Legain, D., & Pino, D. (2014). Land surface spinup for episodic modeling. *Atmos. Chem. Phys.*, *14*(15), 8165–8172.

Bengtsson, L., Andrae, U., Aspelien, T., Batrak, Y., Calvo, J., de Rooy, W., ... others (2017). The HARMONIE–AROME model configuration in the ALADIN–HIRLAM NWP system. *Mon. Wea. Rev.*, *145*(5), 1919–1935.

Bosveld, F. (2019). *Cabauw in-situ observational program 2000 âĂŞ now: Instruments, calibrations and set-up* (Tech. Rep.). Retrieved from http://projects.knmi.nl/cabauw/insitu/observations/documentation/Cabauw_TR/Cabauw_TR.pdf

Davies, H. (1976). A lateral boundary formulation for multi-level prediction models. *Quart. J. R. Meteorol. Soc.*, *102*(432), 405–418.

Deardorff, J. W. (1973). Three-dimensional numerical modeling of the planetary boundary layer. In *Workshop on micrometeorogy, 1973*.

Heinze, R., Dipankar, A., Henken, C. C., Moseley, C., Sourdeval, O., Trömel, S., ... others (2017b). Large-eddy simulations over germany using icon: A comprehensive evaluation. *Quart. J. R. Meteorol. Soc.*, *143*(702), 69–100.

Heinze, R., Moseley, C., Böske, C., Muppa, S., Maurer, V, Raasch, S., & Stevens, B. (2017a). Evaluation of large-eddy simulations forced with mesoscale model output for a multi-week period during a measurement campaign. *Atmos. Chem. Phys.*, *17*, 7083–7109.

Heus, T., van Heerwaarden, C. C., Jonker, H. J. J., Pier Siebesma, A., Axelsen, S., van den Dries, K., ... Vilà-Guerau de Arellano, J. (2010). Formulation of the dutch atmospheric large-eddy simulation (dales) and overview of its applications. , *3*(2), 415–444. Retrieved from https://www.geosci-model-dev.net/3/415/2010/ doi: 10.5194/gmd-3-415-2010

Lund, T. S., Wu, X., & Squires, K. D. (1998). Generation of turbulent inflow data for spatially-developing boundary layer simulations. *Journal of computational physics*, *140*(2), 233–258.

Mayor, S. D., Spalart, P. R., & Tripoli, G. J. (2002). Application of a perturbation recycling method in the large-eddy simulation of a mesoscale convective internal boundary layer. *J. Atmos. Sci.*, *59*(15), 2385–2395.

Mlawer, E. J., Taubman, S. J., Brown, P. D., Iacono, M. J., & Clough, S. A. (1997). Radiative transfer for inhomogeneous atmospheres: Rrtm, a validated correlated-k model for the longwave. *J. Geophys. Res.*, *102*(D14), 16663–16682.

Muñoz-Esparza, D., & Kosović, B. (2018). Generation of inflow turbulence in large-eddy simulations of nonneutral atmospheric boundary layers with the cell perturbation method. *Mon. Wea. Rev.*, *146*(6), 1889–1909.

Muñoz-Esparza, D., Kosović, B., Mirocha, J., & van Beeck, J. (2014). Bridging the transition from mesoscale to microscale turbulence in numerical weather prediction models. *Bound.-Layer Meteor.*, *153*(3), 409–440.

Muñoz-Esparza, D., Kosović, B., Van Beeck, J., & Mirocha, J. (2015). A stochastic perturbation method to generate inflow turbulence in large-eddy simulation models: Application to neutrally stratified atmospheric boundary layers. *Physics of Fluids*, *27*(3), 035102.

Nakayama, H., Takemi, T., & Nagai, H. (2012). Large-eddy simulation of urban boundary-layer flows by generating turbulent inflows from mesoscale meteorological simulations. *Atmospheric Science Letters*, *13*(3), 180–186.

Neggers, R. A. J., Siebesma, A. P., & Heus, T. (2012). Continuous single-column model evaluation at a permanent meteorological supersite. *Bull. Amer. Meteor. Soc.*, *93*(xx), 1389-1400.

Radnóti, G. (1995). Comments on âĂIJa spectral limited-area formulation with time-dependent boundary conditions applied to the shallow-water equationsâĂİ. *Mon. Wea. Rev.*, *123*(10), 3122–3123.

Schalkwijk, J., Jonker, H. J., Siebesma, A. P., & Bosveld, F. C. (2015a). A year-long large-eddy simulation of the weather over cabauw: An overview. *Mon. Wea. Rev.*, *143*(3), 828–844.

Schalkwijk, J., Jonker, H. J., Siebesma, A. P., & Van Meijgaard, E. (2015b). Weather forecasting using gpu-based large-eddy simulations. *Bull. Amer. Meteor. Soc.*, *96*(5), 715–723.

Seifert, A., & Beheng, K. D. (2001). A double-moment parameterization for simulating autoconversion, accretion and selfcollection. *Atmospheric research*, *59*, 265–281.

Seifert, A., & Heus, T. (2013). Large-eddy simulation of organized precipitating trade wind cumulus clouds. *Atmos. Chem. Phys.*, *13*(11), 5631–5645. doi: 10.5194/acp-13-5631-2013

Siebesma, A. P., Bretherton, C. S., Brown, A., Chlond, A., Cuxart, J., Duynkerke, P. G., . . . others (2003). A large eddy simulation intercomparison study of shallow cumulus convection. *J. Atmos. Sci.*, *60*(10), 1201–1219.

Tomassini, L., Field, P. R., Honnert, R., Malardel, S., McTaggart-Cowan, R., Saitou, K., . . . Seifert, A. (2017). The "grey zone" cold air outbreak global model intercomparison: A cross evaluation using large-eddy simulations. *Adv. Model. Earth Syst.*, *9*(1), 39–64.

van Heerwaarden, C. C. (2011). *Surface evaporation and water vapor transport in the convective boundary layer* (Doctoral dissertation, Wageningen University). https://library.wur.nl/WebQuery/wda/1964493.

van Tiggelen, M. (2018). *Towards improving the land- surface-atmosphere coupling in the Dutch Atmospheric Large- Eddy Simulation model (DALES)* (Master's thesis, Delft University of Technology, the Netherlands). https://repository.tudelft.nl/islandora/object/uuid:bbe384d1-3f40-487a-b1a6-7ce34438f2db/datastream/OBJ/download.

Wicker, L. J., & Skamarock, W. C. (2002). Time-splitting methods for elastic models using forward time schemes. *Mon. Wea. Rev.*, *130*(8), 2088-2097.

Wijnant, I. L., van Ulft, B., van Stratum, B. J. H., Barkmeijer, J., Onvlee, J., de Valk, S., C. Knoop, ... Klein Baltink, H. (2019). *The dutch offshore wind atlas (DOWA): description of the dataset* (Tech. Rep.).

Wu, X. (2017). Inflow turbulence generation methods. *Annual Review of Fluid Mechanics*, *49*, 23–49.